Large time behavior and synchronization of complex networks of reaction-diffusion systems of Fitzhugh-Nagumo type

B Ambrosio, M A Aziz-Alaoui, V L E Phan

(2019) Page 1 of 28
doi:xxx000

LARGE TIME BEHAVIOR AND SYNCHRONIZATION OF COMPLEX NETWORKS OF REACTION-DIFFUSION SYSTEMS OF FITZHUGH-NAGUMO TYPE

B. AMBROSIO*

*benjamin.ambrosio@univ-lehavre.fr

M.A. AZIZ-ALAOUI
Normandie Univ, France; ULH, LMAH, F-76600 Le Havre; FR CNRS 3335, 25 rue Philippe Lebon 76600 Le Havre, France

AND

V.L.E. PHAN
An Giang University, Long Xuyen City, An Giang, Vietnam

[Received on 7 January 2019]

We focus on the long time behavior of complex networks of reaction-diffusion systems. In a previous work, we have proved the existence of the global attractor and the L^∞-bound for these networks. Here, we discuss the synchronization phenomenon and establish the existence of a coupling strength threshold value that ensures this synchronization. Then, we apply these results to some particular networks with different structures (i.e. different topologies) and perform numerical simulations. We found out theoretical and numerical heuristic laws for the minimal coupling strength needed for synchronization with respect to the number of nodes and the network topology. We also discuss the link between spatial heterogeneity and synchronization. Our main conclusion is that some of widespread heuristic laws known for synchronization of ODE's, remain valid for networks of RD systems, i.e. networks in which each node, has its own spatial heterogeneity.

Keywords: Complex networks Synchronization Reaction-Diffusion systems FitzHugh-Nagumo.

1. Introduction

Networks of dynamical systems appear naturally in the modeling of numerous applications such as biology, physics, engineering, social networks. Of particular interest are neural networks. There is now evidence that hierarchic structures emerge in the brain. From microscopic to macroscopic scales, they allow to consider the brain as a complex network, see [27, 45]. A first approach is to consider its anatomic connectivity, which describes the physical connections between neurons. After the pioneering works of Golgi and Ramón y Cajal (Nobel Prize in Physiology and Medicine 1906), and the appearance of microscopic techniques, it has been progressively understood (now with elaborate techniques including electrodes or injection of markers), that there exist similar specialized neuronal units organized in densely connected "columns", which are themselves interconnected in order to obtain globally coherent states, see [12]. Obviously, the whole description of nervous system of living organism is only possible for small beings like the nematode Caenorhabditis Elegans (whose nervous system has only 302 neu-

rons). For mammals and especially for humans, a complete description of all the neurons in the brain is until now impossible (indeed, the human brain has 10^{10} neurons and 10^{14} connections). A second approach is to consider functional connectivity. Functional magnetic resonance imaging (fMRI) and electro-physiological recordings brought new insights in functional connections between cortex areas, and functional brain graphs have been constructed from fMRI or electro-physiological recordings, see [12, 45]. Measuring electrical activity has allowed researchers to point out the existence of oscillations characterized by their frequency, amplitude and phase. These characteristics are considered to result from synchronization within a neural ensemble, also referred as local synchronization. In addition to local synchronization, distant neural structures may also synchronize. Indeed, neural oscillations and synchronization have been linked to many cognitive functions such as information transfer, perception, motor control and memory [10, 23, 25, 53]. In this paper, we focus on networks of reaction-diffusion (RD) systems of FitzHugh-Nagumo (FHN) type, that can be seen as neural networks. More precisely, diffusion can be seen as a local connection or diffusion through a single neuron or local neural area whereas the coupling specified by the graph topology corresponds to physical or functional connections at upper scale. Such an idea has been for example exploited in [58, 59], where the authors investigated synchronization on the cortical network of the cat by modeling each node (cortical area) of the network with a small-world sub-network of FHN Ordinary Differential Equations (ODE's). Here, we are interested in the synchronization phenomenon and pattern formation in the whole network of Partial Differential Equations (PDE's). Networks of dynamical systems have attracted a large number of theoretical researches. It is therefore necessary to recall some of them to contextualize our present work. Clearly, our work is somehow related with the dynamical qualitative analysis and pattern formation in networks. A pioneering work in this field is the famous article of Turing [56] on morphogenesis. In this work, Turing points out that an homogeneous stationary solution may be turned instable by adding diffusion terms. It practically provides conditions on coefficients allowing the formation of stationary stable patterns in 2 dimensional RD systems. Some efforts have early been done to extend the Turing pattern formation mechanism to more sophisticated diffusive topologies in networks of ODE's, see [43, 44]. Later, the technique has been applied to large random networks, see [40] and after widely applied for various topologies in different contexts, see [9], and also [7, 8] for stochastic ODE's. Other works rely on networks of ODE's with oscillatory behavior such as the Ginzburg-Landau equations, see [19, 41]. On the other hand numerous papers have dealt with the synchronization phenomenon. The synchronization phenomenon has been studied for a long time and his discovery goes back to Huygens in 1665. For a general presentation of this phenomenon and its analysis we refer to [42, 48], see also [11] for a shorter review. The most widely technique used to study the complete synchronization (i.e. each node of the network is equal asymptotically), is the so called Master Stability Function, which consists to analyze the linearization around the synchronization manifold, see for example [42, 46, 48] and the references therein cited. This technique might provide some insights in our case, however we will adopt here a different point of view. Indeed, our present work distinguishes from the above references on several points. The main point is that we focus in the synchronization of the local nodes which can themselves diffuse. From a theoretical point of view, this means that we consider theoretically, a network of PDE's, (which well-posenedness has been previously established), and we provide a rigorous proof of synchronization in adequate Banach space. More qualitatively, allowing diffusion in each PDE allows us to consider synchronization of patterns, which is a novelty. A discrete analog model would be a network of diffusive subnetworks. In many simulations presented in our work, the emerging patterns correspond to the phase-locking phenomenon of oscillatory systems, which has been widely studied mainly in the case of weak coupling [42]. One can also read [49] for a review within the phase-model approximation (e.g Kuramoto model like), or [6] for a quite exhaustive review of synchronization in

complex networks of oscillators. In our case, the coupling (either diffusive or from the network topology) is not weak, and an interesting tool to track theoretically the pattern formation in this case is the symmetry perspective, [28]. We have obtained relevant results in [**?**] in the case of one single PDE which may be applied to the network. Note also that the patterns which we consider do not generally occur near an unstable stationary solutions. In general they are reached by some particular initial conditions (IC), whereas the homogeneous solution is still stable but not reached by the specified IC . We also consider some patterns obtained in oscillatory-excitable regimes induced by a space inhomogeneity in the PDE coefficients. The choice made here is to use Lyapunov functional to rigorously prove the synchronization phenomenon. This global technique contrasts with the local approaches mentioned above, and applies to all the cases which we will consider. In the previous work [5], we have shown the existence of the global attractor, a set which attracts all the trajectories for large time for the complex network model which we will analyze. This is the set, in which, all the solutions which we effectively observe, lie in. We have also proved the existence of L^∞ bounds. These are fundamental steps which allows us to apply the Lyapunov approach. To summarize, among the very rich literature existing on synchronization of Complex Networks, the present work is one of the first attempt to provide a rigorous proof of synchronization, in networks of PDE's within the Banach space formalism (in [3, 4], we had already considered chains). The theoretical results are illustrated by numerical simulations for particular classes of topologies. Our work, encompasses the synchronization of patterns in the considered PDE's, and show that heuristic laws found in network of ODE's remain valid for the network of PDE's.

Contributions. There are two main contributions in the present paper. First, assuming the existence of the global attractor, we theoretically analyze the synchronization behavior by providing two theorems. The first one gives a general sufficient condition, ensuring identical synchronization. The second one gives a sufficient condition that is more applicable to concrete models. We also give two corollaries for fully connected and ring networks. These corollaries show that the theoretical onset of synchronization follows an inverse power law in the case of the fully connected network and a quadratic law in the case of ring networks regarding the number of nodes. Then, we perform numerical simulations with various initial conditions and study numerically the spatial effects on synchronization and pattern formation for fully connected and ring networks. We obtain heuristic laws of synchronization with respect to the number of nodes that match our theoretical results. This has to be pointed out since the theoretical results give only sufficient conditions whereas numerical simulations seek optimal synchronization threshold values. Also, these laws are not dependent on the different patterns resulting from spatial heterogeneity in IC.

Mathematical framework and preliminaries. First of all, we introduce the mathematical framework we will use throughout this paper. Mathematically speaking, the network is represented by a graph, whose nodes are a d-dimensional RD system and whose edges correspond to the coupling functions between these subsystems. The general system reads as:

$$U_{it} = \tilde{Q}\Delta U_i + \tilde{F}(U_i) + \tilde{H}_i(U_1,...,U_n), i \in \{1,...,n\}. \tag{1.1}$$

In this equation, each variable U_i represents a function from $\Omega \times \mathbb{R}^+$ into $\mathbb{R}^d$, Ω is a bounded domain of $\mathbb{R}^N$ and $\tilde{F} : \mathbb{R}^d \to \mathbb{R}^d$ is the nonlinear reaction term. For all $i \in \{1,...,n\}$, $\tilde{H}_i : \mathbb{R}^{nd} \to \mathbb{R}^d$ is the coupling function between nodes whereas $\tilde{Q}$ is a diagonal matrix of $\mathbb{R}^{d\times d}$ with positive coefficients. If we add boundary conditions to (1.1), we obtain a general reaction-diffusion system. We will not provide details regarding the existence of the semi-group of (1.1), we refer to [34, 35, 55] or [29, 51, 52], for classical results on the existence of semi-group in $L^p(\Omega)$ or in $C^{k,\alpha}(\Omega)$ spaces. A theoretical result on the existence of the global attractor for a particular class of networks of type (1.1) that generalizes the FitzHugh-Nagumo (FHN) equations is given in [5]. Recall that FHN equations are a simplification in

two variables of the HH model of four equations for the action potential propagation in nerve, [24, 31, 39]. A good qualitative analysis of the (FHN) reaction-diffusion system is given in [50], while in [2] we gave a first analysis of a particular network of FHN RD systems. Here, we present results for a network of n partially diffusive systems with d equations. Thus, we assume that we can split the system (1.1) into two subsystems, diffusive and non-diffusive, with respectively s and $d-s$ equations. We allow s to be different from $d-s$[1]. Therefore, we set for all $i \in \{1,...,n\}$, $U_i = (u_i, v_i)$, and write (1.1) in the following way:

$$\left\{ \begin{array}{rcl} u_{it} & = & F(u_i,v_i) + Q\Delta u_i + H_i(u_1,...,u_n), \text{ on } \Omega\times]0,+\infty[, \\ v_{it} & = & -\sigma(x)v_i + \Phi(x,u_i) \text{ on } \Omega\times]0,+\infty[, \end{array} \right. \tag{1.2}$$

where $i \in \{1,...,n\}$, with Neumann Boundary conditions (NBC) on $\partial\Omega$, and where u_i take values in $\mathbb{R}^s$, $1 \leqslant s < d$ whereas v_i take values in $\mathbb{R}^{d-s}$, Q is a diagonal matrix in $\mathbb{R}^{s\times s}$ with coefficients $q^j, j \in \{1,...,s\}$, and H_i take values in $\mathbb{R}^s$. We use the classical notation u_t for $\frac{\partial u}{\partial t}$. This means that diffusion and coupling terms appear only in the s first variables of each subsystem of the network. Finally, $\sigma(x)$ is a diagonal matrix $\mathbb{R}^{(d-s)\times(d-s)}$, with continuous and positive coefficients on $\bar{\Omega}$. We set $\sigma_m = \inf_{i\in\{1,...,d-s\}, x\in\bar{\Omega}} \sigma_{ii}(x)$. We also assume that it has bounded derivatives. The application Φ belongs to $C(\bar{\Omega}) \times C^1(\mathbb{R}^d)$ (and takes values in $\mathbb{R}^{(d-s)}$). When writing explicitly the dependence on x in σ and Φ, we have in mind, a specific version of the FHN RD system which is non-homogeneous in space. Depending, on the value of the constant c, the FHN ODE system may be ocillatory or excitable, see [1–4]. The FHN RD non-homogeneous equation takes advantage of these two properties. This allows to generate a rich behavior. For example, the numerical simulation in figure 7 has been performed with this equation. On the other hand, our proof is not valid in general if Q is x dependent. It can be adapted if H depends on x.

Paper Organization Theoretical results are presented in section 2 and 3. In section 2, we give theoretical results on the synchronization onset of system (1.2) with linear coupling functions. Then, we apply these results to fully connected and ring networks. In section 3, we present numerical simulations for fully connected and unidirectionally coupled ring networks. In these simulations, each node in the graph, is represented by the classical FHN RD system with two equations. Simulations gives an insight on the relation between the number of neurons and the minimal coupling strength needed to reach synchronization. We also pay a particular attention to the effects of spatial dimension. For fully connected networks, our numerical simulations show that the minimal strength value for synchronization follows the inverse power law $\frac{1}{n}$, independently of the patterns induced by initial conditions. In unidirectional coupled ring network, the minimal strength value for synchronization follows a quadratic n^2 law.

2. Synchronization

We assume the existence of the global attractor and L^∞-bounds. This result has been published in [5]. In particular, we assume that there exists a positive constant m_∞ such that for time large enough $||U||_\infty < m_\infty$. Therefore, we can deal with synchronization of solutions within this attractor. We focus on this ubiquitous phenomenon and restrict ourselves to identical synchronization in networks with linear coupling. We determine sufficient coupling strength values, ensuring identical synchronization in complex network (1.2). We refer, for example to [11, 17, 21, 22, 37, 48, 54], for relevant works

[1] In the FHN equation, since there is one diffusive equation and one non-diffusive, $s = d-s$. In general, in neuron models inspired from the *HH* equations, the diffusion appears only in the first equation which corresponds to the membrane potential. The other equations being related to the gating variables. Our analysis allows s to be different of $d-s$ as in the case of the *HH* equation or in the Hindmarsh-Rose diffusive model.

on the synchronization phenomenon. These values are related to the number of nodes, the coupling configuration and the properties of each subsystem. Note that these results hold when patterns with spatial heterogeneity occur in each PDE of the network. This point will be discussed in more details in the last section. As far as we know, only a few works deal with synchronization for PDE's, see [32, 57]. Technically, to establish the synchronization, we exhibit a Lyapunov function for the network. Since we assume L^∞-bounds as obtained in the previous work [5], it is always possible to find such a Lyapunov function provided that the coupling strength is large enough. The ODE case has been studied (see [13, 14]). Like there, we assume that the connectivity matrix has zero row and column sums. We extend the results known in the ODE case to networks of RD systems. We find out threshold synchronization values, see theorems 2.2 and 2.3 which indicate that the laws exhibited in the ODE case remain valid. The rich behavior allowed by the fact that each node can diffuse, in a spatial domain will be illustrated in the third section.

DEFINITION 2.1 (see [2]) Let $U(t) = (U_1(t), U_2(t), ..., U_n(t))$ be a network with a given topology. We say that U synchronizes identically if,

$$\lim_{t\to+\infty} \sum_{i=1}^{n-1} |U_i(t) - U_{i+1}(t)|_{2,\Omega} = 0.$$

where notation is that of (1.2) with $U_i = (u_i, v_i)$.

We consider the network,

$$\left\{ \begin{array}{lcl} u_{it} & = & F(u_i, v_i) + Q\Delta u_i + \sum_{k=1}^n c_{ik} u_k, \quad i \in \{1, ..., n\} \\ v_{it} & = & -\sigma(x) v_i + \Phi(x, u_i), \end{array} \right. \tag{2.1}$$

with Neumann Boundary conditions on $\partial\Omega$, which is a particular case of (1.2), where :

$$H_i(u_1, ..., u_n) = \sum_{k=1}^n c_{ik} u_k.$$

We will assume that the matrix $G = (c_{ik})_{1\leqslant i,k\leqslant n}$ has vanishing row and column-sums and non-negative off-diagonal elements, i.e., $c_{ik} \geqslant 0$ for $i \neq k$, and

$$c_{ii} = -\sum_{k=1, k\neq i}^n c_{ik} = -\sum_{k=1, k\neq i}^n c_{ki}. \tag{2.2}$$

Note that the zero sum row asumption corresponds to diffusive coupling, since in this case, we have $\sum_{k=1}^n c_{ik} u_k = \sum_{k=1, k\neq i}^n c_{ik}(u_k - u_i)$. Assuming diffusive coupling, the zero sum column asumption means that the sum of incoming coefficients balances the outgoing coefficients and it is referred as node balance property. This last one can be relaxed, see [15], for the ODE case.

The connectivity matrix G defines the graph topology as well as the coupling strength between nodes. Indeed, there is an edge between node i and node k if and only if $c_{ik} > 0$. We consider here an arbitrary connected and directed network of linearly coupled RD systems satisfying (2.2). Obviously, symmetric networks with vanishing row-sums are a particular case of the one considered here. Before going more into details, let us summarize the main ideas of this section. We establish the synchronization result in theorem 2.2 which relies on the statement of a Lyapunov function $\mathscr{V}$ that reads as the sum of the norms of all vectors $U_i - U_j$. The first step is to exhibit a positive number a that annihilates the

effects of nonlinear terms of (2.1); this is done in lemma 2.1, then the proof follows from computations that use equation (2.2), which itself involves all the pairs (i,j) in $\mathscr{V}$. However, the result of theorem 2.2 can not be applied directly to concrete networks. This is the purpose of theorem 2.3, which gives a sufficient condition for synchronization applicable in networks with an arbitrary topology. Its proof relies on the computation of the sum of all minimal lengths joining any pair of nodes passing through a given edge of the graph, see [13, 14]. This idea comes from lemma 2.2 which bounds all terms in the left hand side of (2.5) (in which all the pairs (i,j) appear) by terms of the right hand side (only the pairs (i,j) corresponding to non zero coupling, $c_{ij} \neq 0$, i.e. edges of the graph, appear).

We start with lemma 2.1. It establishes the existence of a positive number a that annihilates the effects of nonlinear terms. Let us denote by X an arbitrary vector of $\mathbb{R}^d$, X_s the vector of the s first coordinates, X_{d-s}, the vector of the $d-s$ last coordinates of X, and $||\cdot||$ the vectorial euclidian norm or its subordinate matricial norm. We also denote DF the $s \times d$ Jacobian matrix of F, and $D\Phi$ the $(d-s)\times s$ Jacobian matrix of F with respect to the u variable.

LEMMA 2.1 For each solution $(U_1, U_2, ..., U_n)$ of (2.1), there exists a time T, a positive constant κ and a positive number a, such that for all $t > T$, for all $X \in \mathbb{R}^d$, and for all $i, j \in \{1, ..., n\}$,

$$\begin{array}{c} X_s.\left[\int_0^1 DF(\theta U_j + (1-\theta)U_i)d\theta\right]X + \\ X_{d-s}.\left(-\sigma(x)X_{d-s} + \left[\int_0^1 D\Phi(\theta u_j + (1-\theta)u_i)d\theta\right]X_s\right) - a||X_s||^2 \quad \leqslant -\kappa||X_{d-s}||^2. \end{array}$$

Proof. We have:

$$\begin{array}{c} X_s.\left[\int_0^1 DF(\theta U_j + (1-\theta)U_i)d\theta\right]X + \\ X_{d-s}.\left(-\sigma(x)X_{d-s} + \left[\int_0^1 D\Phi(\theta u_j + (1-\theta)u_i)d\theta\right]X_s\right) \\ \leqslant M_1||X_s||||X|| - \sigma_m||X_{d-s}||^2\sum_{i=1}^s + M_2||X_{d-s}||||X_s|| \\ \leqslant M_1||X_s||^2 + M_1||X_s||||X_{d-s}|| + M_2||X_{d-s}||||X_s|| \end{array}$$

where

$$M_1 = \sup_{||U||_\infty < m_\infty} ||DF(U)||$$

and similarly

$$M_2 = \sup_{||u||_\infty < m_\infty} ||D_u\Phi(u)||.$$

By using Young's inequality $\alpha\beta \leqslant \frac{\alpha^2}{2\varepsilon} + \varepsilon\frac{\beta^2}{2}$, with $\varepsilon = \frac{2M_1}{\sigma_m}, \alpha = ||X_{d-s}||, \beta = ||X_s||$ and with $\varepsilon = \frac{2M_2}{\sigma_m}, \alpha = ||X_{d-s}||, \beta = ||X_s||$ we obtain,

$$\begin{array}{c} X_s.\left[\int_0^1 DF(\theta U_j + (1-\theta)U_i)d\theta\right]X + \\ X_{d-s}.\left(-\sigma(x)X_{d-s} + \left[\int_0^1 D\Phi(\theta u_j + (1-\theta)u_i)d\theta\right]X_s\right) \\ \leqslant -\frac{\sigma_m}{2}||X_{d-s}||^2 + \frac{M_1^2+M_2^2}{2}||X_s||^2 \end{array}$$

which gives the result with

$$\kappa = \frac{\sigma_m}{2} \text{ and } a = \frac{M_1^2 + M_2^2}{\sigma_m}.$$

□

Now, we present the main result that provides sufficient conditions for identical synchronization. To this aim, we introduce the following notations: for all $i, j \in \{1, ..., n\}$,

$$w_{ij} = u_j - u_i, \quad z_{ij} = v_j - v_i, \quad \varepsilon_{ij} = \frac{c_{ij} + c_{ji}}{2}, \tag{2.3}$$

and

$$w_{ijt} = \frac{d}{dt} w_{ij}, \quad z_{ijt} = \frac{d}{dt} z_{ij}. \tag{2.4}$$

THEOREM 2.2 If we assume that

$$\frac{a}{n} \sum_{i<j} |w_{ij}|^2_{2,\Omega} < \sum_{i<j} \varepsilon_{ij} |w_{ij}|^2_{2,\Omega} \tag{2.5}$$

where $a > 0$ is given by lemma 2.1, then the system (2.1) synchronizes in the sense of definition 2.1.

Proof. We split G into the sum of two matrices E and L, which are symmetric and antisymmetric, with E being $(\varepsilon_{ik}), i, k \in \{1, ..., n\}$ and L being $(\delta_{ik}), i, k \in \{1, ..., n\}$, *i.e.* :

$$G = E + L, \tag{2.6}$$

where,

$$\delta_{ik} = \frac{1}{2}(c_{ik} - c_{ki}). \tag{2.7}$$

One can easily check that both matrices E and L have zero row sums. Since $w_{ij} = u_j - u_i$, $z_{ij} = v_j - v_i, i, j \in \{1, ..., n\}$, we obtain,

$$\begin{cases} w_{ijt} = & F(u_j, v_j) - F(u_i, v_i) + Q\Delta w_{ij} + \sum_{k=1}^n (\varepsilon_{jk} w_{jk} - \varepsilon_{ik} w_{ik} + \delta_{jk} w_{jk} - \delta_{ik} w_{ik}), \\ z_{ijt} = & -\sigma(x) z_{ij} + \Phi(x, u_j) - \Phi(x, u_i). \end{cases}$$

Moreover,

$$\begin{aligned} F(u_j, v_j) - F(u_i, v_i) = & \int_0^1 \frac{d}{d\theta} F(\theta U_j + (1-\theta) U_i) d\theta \\ = & \left[\int_0^1 DF(\theta U_j + (1-\theta) U_i) d\theta \right] (U_j - U_i), \end{aligned}$$

and,

$$\Phi(x, u_j) - \Phi(x, u_i) = \int_0^1 \frac{d}{d\theta} \Phi(\theta u_j + (1-\theta) u_i) d\theta = \left[\int_0^1 D\Phi(\theta u_j + (1-\theta) u_i) d\theta \right] w_{ij}.$$

Hence, we can write,

$$\begin{cases} w_{ijt} & = \left[\int_0^1 DF(\theta U_j + (1-\theta) U_i) d\theta \right] (U_j - U_i) + Q\Delta w_{ij} + \\ & \quad \sum_{k=1}^n (\varepsilon_{jk} w_{jk} - \varepsilon_{ik} w_{ik} + \delta_{jk} w_{jk} - \delta_{ik} w_{ik}), \\ z_{ijt} & = -\sigma(x) z_{ij} + \left[\int_0^1 D\Phi(\theta u_j + (1-\theta) u_i) d\theta \right] w_{ij}. \end{cases} \tag{2.8}$$

where $i, j \in \{1, ..., n\}$. Now, let us introduce the following function:

$$\mathscr{V}(t) = \sum_{i=1}^{n} \sum_{j=1}^{n} \left(|w_{ij}|^2_{2,\Omega} + |z_{ij}|^2_{2,\Omega} \right). \tag{2.9}$$

In order to reach synchronization, it is sufficient to find conditions ensuring that $\mathscr{V}$ is a Lyapunov function with negative orbital derivative. Since the graph is connected, it would be natural to include in $\mathscr{V}$, only the terms w_{ij} corresponding to non-zero coefficients ε_{ij}. However, as we will see, including all terms w_{ij} in $\mathscr{V}$ will allow specific computations leading to the result.

$$\begin{aligned}
\frac{1}{2}\frac{d}{dt}\mathscr{V} &= \sum_{i=1}^{n}\sum_{j=1}^{n}\int_{\Omega}(w_{ij}.w_{ijt} + z_{ij}.z_{ijt}) \\
&= \sum_{i=1}^{n}\sum_{j=1}^{n}(\int_{\Omega} w_{ij}.(\left[\int_0^1 DF(\theta U_j + (1-\theta)U_i)d\theta\right](U_j - U_i) + Q\Delta w_{ij} \\
&\quad + \sum_{k=1}^{n}(\varepsilon_{jk}w_{jk} - \varepsilon_{ik}w_{ik} + \delta_{jk}w_{jk} - \delta_{ik}w_{ik})) \\
&\quad + \int_{\Omega} z_{ij}.(-\sigma(x)z_{ij} + \left[\int_0^1 D\Phi(\theta u_j + (1-\theta)u_i)d\theta\right] w_{ij})).
\end{aligned}$$

By lemma 2.1, there exist positive constants a and κ such that,

$$\begin{aligned}
\frac{1}{2}\frac{d\mathscr{V}}{dt} \leqslant & \sum_{i=1}^{n}\sum_{j=1}^{n}\left(a\int_{\Omega}||w_{ij}||^2 - \kappa\int_{\Omega}||z_{ij}||^2 + \int_{\Omega} w_{ij}.Q\Delta w_{ij}\right) \\
& + \sum_{i=1}^{n}\sum_{j=1}^{n}\left(\int_{\Omega} w_{ij}.\left(\sum_{k=1}^{n}(\varepsilon_{jk}w_{jk} - \varepsilon_{ik}w_{ik})\right) + \int_{\Omega} w_{ij}.\left(\sum_{k=1}^{n}(\delta_{jk}w_{jk} - \delta_{ik}w_{ik})\right)\right)
\end{aligned}$$

Now, let us remark that, thanks to Green's formula, we have that for all i, j the component $w_{ij,k}$ satisfies,

$$\int_{\Omega} w_{ij,k}\Delta w_{ij,k}dx = -\int_{\Omega}||\nabla w_{ij,k}dx||^2 + \int_{\delta\Omega} w_{ij,k}\nabla w_{ij,k}\vec{n}dx$$

where $\vec{n}$ denotes the normal unitary vector at a point x on the boundary of Ω. Assuming Neumann boundary conditions $\nabla w_{ij,k}\vec{n} = 0$ on $\delta\Omega$, we have, for all $i, j \in \{1, .., n\}$,

$$\int_{\Omega} w_{ij}.Q\Delta w_{ij} = -\sum_{k=1}^{s}\int_{\Omega}||\nabla w_{ij,k}||^2.$$

It follows that,

$$\begin{aligned}
\tfrac{1}{2}\tfrac{d\mathscr{V}}{dt} \leqslant & \sum_{i=1}^{n}\sum_{j=1}^{n}\left(a\int_{\Omega}||w_{ij}||^2 - \kappa\int_{\Omega}||z_{ij}||^2\right) \\
& + \sum_{i=1}^{n}\sum_{j=1}^{n}\left(\int_{\Omega} w_{ij}.\left(\sum_{k=1}^{n}(\varepsilon_{jk}w_{jk} - \varepsilon_{ik}w_{ik})\right) + \int_{\Omega} w_{ij}.\left(\sum_{k=1}^{n}(\delta_{jk}w_{jk} - \delta_{ik}w_{ik})\right)\right)
\end{aligned}$$

The last term of the second line in the above equation vanishes. Indeed, writing $w_{jk} = w_{ji} + w_{ik}$ and using $\sum_{k=1}^{n} \delta_{jk} = 0$, we obtain,

$$\begin{aligned}\sum_{i,j,k=1}^{n} w_{ij}.\big(\delta_{jk}w_{jk} - \delta_{ik}w_{ik}\big) = &\quad 2\textstyle\sum_{i,j,k=1}^{n} w_{ij}.\delta_{jk}w_{ik} \\ = &\quad 2\textstyle\sum_{i,j}^{n} \delta_{jj}||w_{ij}||^2 + 2\sum_{i,j=1}^{n}\sum_{k\neq j} \delta_{jk}w_{ij}.w_{ik}.\end{aligned}$$

Obviously, since $\delta_{jj} = 0$,

$$\sum_{i,j}^{n} \delta_{jj}||w_{ij}||^2 = \quad 0.$$

Moreover, since $\delta_{jk} = -\delta_{kj}$, we have, for all $i \in \{1,...,n\}$,

$$\sum_{j=1}^{n}\sum_{k\neq j} \delta_{jk}w_{ij}.w_{ik} = 0.$$

Now, we deal with the other terms. We have:

$$\begin{aligned}\sum_{i=1}^{n}\sum_{j=1}^{n} w_{ij}.\sum_{k=1}^{n}(\varepsilon_{jk}w_{jk} - \varepsilon_{ik}w_{ik}) &= \sum_{i,j,k=1}^{n} \varepsilon_{jk}w_{ij}.w_{jk} - \sum_{i,j,k=1}^{n} \varepsilon_{ik}w_{ij}.w_{ik} \\ &= \sum_{i,j,k=1}^{n} \varepsilon_{jk}w_{ij}.w_{jk} - \sum_{i,j,k=1}^{n} \varepsilon_{jk}w_{ji}.w_{jk} \\ &= 2\sum_{i,j,k=1}^{n} \varepsilon_{jk}w_{ij}.w_{jk} \\ &= 2\sum_{i,j,k=1}^{n} \varepsilon_{jk}(w_{ik}.w_{jk} - ||w_{kj}||^2),\end{aligned}$$

since $w_{ij} = w_{ik} + w_{kj}$. Moreover,

$$\begin{aligned}\sum_{i,j,k=1}^{n} w_{ik}.\varepsilon_{jk}w_{jk} &\leqslant \sum_{i,j,k=1}^{n} \frac{1}{2}\varepsilon_{jk}(||w_{ik}||^2 + ||w_{jk}||^2) \\ &= \frac{1}{2}\sum_{i,k=1}^{n} ||w_{ik}||^2 \sum_{j=1}^{n} \varepsilon_{jk} + \frac{n}{2}\sum_{j,k=1}^{n} \varepsilon_{jk}||w_{jk}||^2 \\ &= \frac{n}{2}\sum_{j,k=1}^{n} \varepsilon_{jk}||w_{jk}||^2,\end{aligned}$$

since $\sum_{j=1}^{n} \varepsilon_{jk} = 0$. Hence, we have:

$$\sum_{i=1}^{n}\sum_{j=1}^{n} w_{ij}.\sum_{k=1}^{n}(\varepsilon_{jk}w_{jk} - \varepsilon_{ik}w_{ik}) \leqslant -n\sum_{j,k=1}^{n} \varepsilon_{jk}||w_{jk}||^2$$

Finally, we obtain:

$$\begin{aligned}
\tfrac{1}{2}\tfrac{d\mathscr{V}}{dt} &\leqslant \sum_{i,j=1}^{n}(a|w_{ij}|^2_{2,\Omega}-\kappa|z_{ij}|^2_{2,\Omega})-n\sum_{j,k=1}^{n}(\varepsilon_{jk}|w_{jk}|^2_{2,\Omega}\\
&= 2\sum_{i<j}(a|w_{ij}|^2_{2,\Omega}-\kappa|z_{ij}|^2_{2,\Omega})-2n\sum_{i<j}\varepsilon_{ij}|w_{ij}|^2_{2,\Omega}\\
&\leqslant -2\kappa\sum_{i<j}|z_{ij}|^2_{2,\Omega}+2a\sum_{i<j}|w_{ij}|^2_{2,\Omega}-2n\sum_{i<j}^{n}\varepsilon_{ij}|w_{ij}|^2_{2,\Omega}\\
&< 0,
\end{aligned}$$

thanks to hypothesis (2.5). □

Now, we want to prove theorem 2.3 which gives a sufficient condition for synchronization which can be applied for concrete networks. Theorem 2.2 requires (2.5) to be satisfied for all time to ensure synchronization. What is somehow strange in (2.5) is that in the left-hand side, all the variables w_{ij} appear while in the right-hand side, due to the parameters ε_{ij}, only variables corresponding to existing edges appear. The following lemma provides a key element of the proof of the theorem . It allows to obtain a bound with only terms corresponding to edges, by introducing paths between all pair of nodes. This will allow to obtain a concrete condition ensuring (2.5), and provide the key element of .

LEMMA 2.2 For all $i,j\in\{1,...,n\}$, and for all sequences, $(i_l)_{l\in\{0,...,k\}}$, with $k\in\{0,...,n\}$ and $i_0=i,...,i_k=j$, we have:

$$||w_{ij}||^2\leqslant k(\sum_{l=0}^{k-1}||w_{i_li_{l+1}}||^2). \tag{2.10}$$

Proof. We write:

$$\begin{aligned}
||w_{ij}||^2 &= ||\sum_{l=0}^{k-1}w_{i_li_{l+1}}||^2\\
&= (\sum_{l=0}^{k-1}w_{i_li_{l+1}}).(\sum_{l=0}^{k-1}w_{i_li_{l+1}})\\
&= \sum_{l=0}^{k-1}||w^2_{i_li_{l+1}}||+2\sum_{l<m}w_{i_li_{l+1}}w_{i_mi_{m+1}}\\
&\leqslant k\sum_{l=0}^{k-1}||w_{i_li_{l+1}}||^2 \quad \text{by using Young's inequality.}
\end{aligned}$$

□

Note that the lemma is valid for an arbitrary sequence, but we will use it for sequences corresponding to edges in the graph.

Without caring about edge direction in the graph, for each (i,j), $i<j$, we choose a unique path of minimal length in the graph joining nodes i and j. We denote this path P_{ij}, $l(P_{ij})$ its length, and its nodes by: $(i_l)_{l\in\{0,...,length(P_{ij})\}}$, with $i_0=i,...,i_{length(P_{ij})}=j$. For each (k,l), $k<l$ corresponding to an edge in the graph (i.e. $\varepsilon_{kl}\neq 0$), we define α_{kl} as the sum of all the lengths of the minimal paths passing through the edge (k,l). If (k,l) is not an edge of the graph, we set $\alpha_{kl}=0$:

$$\alpha_{kl}=\begin{cases}\sum_{i<j,(k,l)\in P_{ij}}length(P_{ij}) \text{ if } (k,l) \text{ is an edge of the graph,}\\ 0 \text{ if } (k,l) \text{ is not an edge of the graph.}\end{cases} \tag{2.11}$$

Figure 1 gives an example of the computation of these coefficients.

THEOREM 2.3 Let us assume that for each edge (k,l), we have,

$$\frac{a}{n}\alpha_{kl} < \varepsilon_{kl},$$

then the system (2.1) synchronizes in the sense of definition 2.1.

Proof. Now, the proof of theorem 2.3 follows from theorem 2.2 and lemma 2.2. We have,

$$\begin{aligned}\sum_{i<j}||w_{ij}||^2 &\leqslant \sum_{i<j} length(P_{ij}) \sum_{l=0}^{length(P_{ij})-1} ||w_{i_l i_{l+1}}||^2 \text{ thanks to lemma 2.2} \\ &= \sum_{k<l}\alpha_{kl}||w_{kl}||^2 \text{ by reordering the terms of the sum along the edges of the graph.}\end{aligned}$$

The result follows then from theorem 2.2. □

REMARK 2.1 We recover here results found in [13, 14] for ODE systems. Hence, our proof, establishes that these results known in the ODE case remain valid for the RD case presented here. In the RD networks, however, each node has its own spatial heterogeneity. This allows a much more richer behavior than the ODE case. Numerical simulations in the third part will illustrate this point.

COROLLARY 2.1 (Fully connected network) We assume that $\forall i,j \in \{1,...,n\}$, $i \neq j$ $\varepsilon_{ij} > \frac{a}{n}$, then (2.1) synchronizes in the sense of definition 2.1.

Proof. This result comes obviously from theorem 2.3, since for fully connected network, $\alpha_{ij} = 1$. Note that in the particular case of a fully connected network, we could also obtain this corollary from theorem 2.2. □

COROLLARY 2.2 (Unidirectionally ring network) We assume that the connectivity matrix $G = (c_{ij}), 1 \leqslant i,j \leqslant n$, is given by $c_{ii} = -c < 0\ \forall i \in \{1,...,n\}$, $c_{ii+1} = c_{n1} = c\ \forall i \in \{1,...,n-1\}$, and $c_{ij} = 0$ otherwise. Then, if we assume that

$$c > \begin{cases} \frac{a}{12}(n^2-1) & \text{if} \quad n \text{ odd} \\ \frac{a}{12}(n^2+2) & \text{if} \quad n \text{ and } \frac{n}{2} \text{ even} \\ \frac{a}{12}(n^2+8) & \text{if} \quad n \text{ even and } \frac{n}{2} \text{ odd} \end{cases}$$

the network (2.1) synchronizes in the sense of definition 2.1.

Proof. We start with the case of n odd. For each pair of nodes of the graph, there is a unique path of minimal length joining the nodes. If we suppose that $n = 2k+1$, then for each node indexed by l:

$$\begin{aligned}\alpha_{ll+1} &= (1+...+k)+(2+....+k)+...+(k-1+k)+k \\ &= \textstyle\sum_{i=1}^{k}\sum_{j=i}^{k} j \\ &= \frac{(n-1)(n+1)n}{24}.\end{aligned}$$

The figure 2-a gives an example of such a network. In the case where of n even, we assume that $n = 2k$. For each pair of nodes (i,j) in the graph, if the distance between i and j is less than k, there exists a unique path of minimal length joining the nodes. But if the distance between i and j is equal to k, there exists two distinct paths of minimal length joining the nodes. Therefore, we can choose for each pair

(i, j) of distance k, alternatively the minimal path through the left and through the right (i.e. for example, for node 1, the minimal path of length k through the left). Then we find, if $\frac{n}{2}$ is even,

$$\begin{aligned}\alpha_{ll+1} &= (1+...+k)+(2+....+k-1)+...+(k-1+k)+k-1\\ &= \sum_{i=1}^{k}\sum_{j=i}^{k} j-\frac{k}{2}k\\ &= \frac{n(n^2+2)}{24}.\end{aligned}$$

Figure 2-b gives an example of such a network. If $\frac{n}{2}$ is odd and in the worst case,

$$\begin{aligned}\alpha_{ll+1} &= (1+...+k)+(2+....+k-1)+(3+....+k)+...+(k-1)+k\\ &= \sum_{i=1}^{k}\sum_{j=i}^{k} j-\frac{k-1}{2}k\\ &= \frac{n(n^2+8)}{24}.\end{aligned}$$

□

REMARK 2.2 Le us make a remark on the computation of the coefficient a, introduced in lemma 2.1. It can be evaluated in each concrete case. For example, in the FHN case which we will consider in numerical simulations (with the cubic $f(u) = -u^3 + 3u$), the coefficient a can be obtained thanks to a bound on $f'(u) = 3(1-u^2)$. It is observed numerically, that u remains bounded in a specific region (see for example [1, 2, 4]). Using this fact, one can provide a roughly bound of 10 for the coefficient a. This is (much) greater than the bound which will be numerically observed in examples in the next section.

REMARK 2.3 Note that theorem 2.2 and 2.3 are valid for directed, undirected and weighted topologies. In the manuscript, for the fully connected network, corollary 2.1 provides the following sufficient condition for synchronization:

$$\varepsilon_{ij} > \frac{a}{n}.$$

If the network is undirected, then, $\varepsilon_{ij} = \frac{c_{ij}+c_{ji}}{2} = c_{ij}$, and the condition reads $\forall i, j, c_{ij} > \frac{a}{n}$. If the network is directed, and if we allow only one directionnal edge for each couple of nodes, then either $c_{ij} = 0$ or $c_{ji} = 0$. Then the condition reads $\forall i, j, c_{ij} > 2\frac{a}{n}$ or $c_{ji} > 2\frac{a}{n}$. Note that these conditions are valid for weighted networks as well. In the case of the ring network, corollary 2.2 provides the sufficient condition

$$c > \frac{a}{12}(n^2-1),$$

for unidirectionally non-weighted topologies (odd case). Applying the previous computation for undirected graphs would lead to the condition $c > \frac{a}{24}(n^2-1)$. For unidirectionnaly weighted graphs, it would read:

$$\forall i, c_{i,i+1} > \frac{a}{12}(n^2-1).$$

3. Numerical simulations

In this section, we consider networks of type (2.1) with:

$$\begin{aligned} d = 2, s = 1,\\ F(u,v) = \frac{1}{\varepsilon}(-u^3+3u-v), Q = \frac{d_u}{\varepsilon}\\ \sigma(x) = b, \quad \Phi(x,u) = au+c,\end{aligned}$$

i.e. each node is represented by the following reaction-diffusion system of FitzHugh-Nagumo type,

$$\begin{cases} \varepsilon u_t = d_u \Delta u - u^3 + 3u - v \quad \text{on } \Omega \times \mathbf{R}^+ \\ v_t = au - bv + c(x) \qquad \text{on } \Omega \times \mathbf{R}^+ \end{cases} \tag{3.1}$$

where $u = u(x,t), v = v(x,t)$, $d_u, a, b > 0$, $\Omega \subset \mathbf{R}^N$ (in our numerical simulations, $N = 2$) is a regular bounded open set, and with Neumann zero flux conditions on the boundary.

We perform numerical simulations in two cases: fully connected networks in one hand and unidirectionally coupled ring networks in the other hand, both with linear coupling. As far as we know, only few results exist for networks of reaction-diffusion systems; the case of a chain network has been partially investigated in [2]. As we have mentioned before, a specifity of our work is that each node may have his own spatial heterogeinity. We use two ways to induce asymptotic space heterogeneity. One way is to choose specific IC. The other is to choose c as a spatial-dependent function.

We use the following parameter values:

$$a = 1, b = 0.001, \varepsilon = 0.1, d_u = 0.05. \tag{3.2}$$

The numerical integration of the network has been done thanks to our own C^{++} program, on a square domain Ω. For discretization in space we used a finite difference method with a space step of 0.5. For the time integration, we used a Runge-Kutta 4 scheme with a time step of 0.001. The main concern of this section is to investigate:

- The existence of heuristic laws for the network synchronization with respect to the number of nodes in the graph. This means that we seek to write the threshold synchronization values as functions of the number of nodes in the networks.
- The influence of spatial heterogeneity in each node with respect to the synchronization phenomenon.

Our main conclusion are summed up in the following results:

- There exists heuristic laws of coupling strength with respect to the number of nodes in the graph, which are in agreement with the theoretical results of section 2 and with known laws for ODE networks.
- Spatial heterogeneity in each node, inducing various kind of patterns, does not affect these heuristic laws.

As it has been done for ODE's, see for example [13, 14] or [17, 18] in case of the Hindmarsh-Rose model and in agreement with the theoretical results of section 2, the threshold value for synchronization is given by an inverse power law $\frac{1}{n}$ in the case of fully connected networks, and a quadratic law n^2 in the case of a ring networks. We first deal with the fully connected network in the first subsection, and then, with the unidirectional ring network in the second subsection.

3.1 *Fully connected network*

For the fully connected network, the system reads as:

$$\begin{cases} \varepsilon u_{it} = -u_i^3 + 3u_i - v_i + d_u \Delta u_i - g_n \displaystyle\sum_{j=1, j\neq i}^{n} (u_i - u_j) \qquad i = \overline{1,n}, \\ v_{it} = au_i - bv_i + c(x) \end{cases} \tag{3.3}$$

where g_n is the constant coupling strength between each pair of nodes in the graph. We comment hereafter the numerical simulations illustrated in figures 3-9 below. The table 1 summarizes the detailed heuristic laws found numerically.

The case $c(x) = 0$

Initial conditions with approximately half of spirals and half of homogeneous

- In figure 3, we present the evolution of the coupling strength value g_n needed for synchronization with respect to the number of nodes in the graph in the case $c = 0$. We consider half of nodes with initial conditions (IC) leading to spirals and half of nodes leading to homogeneous (constant in space) solutions. We vary the number of nodes from three to twenty. We obtain a heuristic inverse power law in $\frac{1}{n}$. This is in good agreement with our theoretical results. The spatial effects considered here do not affect this widespread heuristic law found for ODE's (i.e. non space dependents) fully connected networks.

- Figure 4, represents a dot of the previous inverse curve, for $n = 3$, in order to exhibit the pattern evolution up to the onset of synchronization; we choose two spiral IC and one homogeneous. We plot the synchronization error between nodes, for different coupling values, and also the spiral patterns observed for each node. Simulations show that synchronization occurs for a threshold value of $g_3 \simeq 0.015$. We can see that asymptotically all the nodes evolve as spiral patterns.

Random initial conditions in $[-1,1]$

- Figure 5 is analog to figure 4 but with different IC. Here, for each $x \in \Omega$, we choose $u_i(x,0)$ and $v_i(x,0)$, $i \in \{1,3\}$ as equal random uniform values in $[-1,1]$. IC $u_2(x,0)$ and $v_2(x,0)$ are set to 0. Note that choosing an interval centered in 0 is crucial here to obtain multiple spiral patterns of figure 4, this relies on the symmetry of the FHN system, see [4]. The simulations show synchronization for a threshold value of $g_3 \simeq 0.014$. They also asymptotically show three matched multiple spiral patterns (noly two are shown since node 3 and node 1 have the same behavior by symmetry).

The case $c(x) \neq 0$

- In figure 6, we show the synchronization of a fully connected network (3.3) with $n = 3$, and $c(x)$ a non constant function such that $c(x) = 0$ if x is in a small neighborhood of $(0,0)$, and $c(x) = -1.1$ otherwise. For one subsystem, and thanks to its oscillatory-excitable property, the FHN system generates propagating periodic pulses starting at $(0,0)$, see also [1]. For IC, we choose three distinct space-homogeneous values. We observe that synchronization occurs for $g_3 \geqslant 0.005$. Asymptotically, the three subsystems generate matching propagating concentric rings.

- In figure 7, we illustrate the time evolution of fixed central cells and peripheral cells of simulation considered in figure 6. It shows spike synchronization and complicated mixed mode oscillations. Note, that the case of two coupled slow-fast FHN ODE systems has been investigated in [33]. However, since we consider her PDE's, the phenomenon illustrated here is more sophisticated.

Auxiliary observations

- In figure 8, we show a possible effect of a lack of symmetry in IC. This figure has to be compared with figure 5, since only the value of $(u_2(0,0), v_2(0,0))$ differs here. Its value is set to $(1,1)$

IC	$c(x)=0$	$c(x)\neq 0$
H	$\frac{0.0288}{n}+0.0004$	$\frac{0.015}{n}+0.0004$
S+H	$\frac{0.046}{n}-0.00043$	$\frac{0.02205}{n}+0.00185$
RU1+H	$\frac{0.0429}{n}-0.00129$	$\frac{0.0193}{n}-0.00043$
RU2+H	$\frac{0.07098}{n}-0.00016$	$\frac{0.0194}{n}+0.0005375$
S	$\frac{0.03}{n}$	$\frac{0.02496}{n}-0.00032$
RU2	$\frac{0.096}{n}+0.006$	$\frac{0.0288}{n}+0.0004$

Table 1. Fully connected network. Heuristic laws of synchronization threshold values with respect to the number of nodes in fully connected networks. We choose different kind of IC leading to several patterns. All the simulations show the emergence of the widespread inverse power law. The abbreviations are the following: IC= initial conditions, H= space homogeneous, S= spirals, RU1= random uniform law on $[0,1]$, RU2= random uniform law on $[-1,1]$, S+H= approximately half of S and half of H. $c(x)\neq 0$ means $c(x)=0$ at center and $c(x)=-1.1$ otherwise.

instead of $(0,0)$ in figure 5. As we have pointed out in [2, 4], symmetry allows us to obtain patterns in FHN system. Thus, choosing IC with random uniform law in $[-1,1]$ in one FHN model leads to multiple spirals. But if we choose random uniform law in $[0,1]$, we obtain space homogeneous solutions. In fact,"almost all IC" lead to solutions homogeneous in space, see [2, 4]. This fact has to be linked with Peskin conjecture (1975), see [47], made for two integrate and fire coupled oscillator models: "for identical oscillators and almost all initial conditions the system approaches a state in which all oscillators are firing synchronously". Here, changing the IC $(u_2(0,0),v_2(0,0))$, leads to the loose of multiple spiral patterns.. The network synchronizes but with other patterns.

- In figure 9, we show the evolution of the coupling strength value g_{20} needed for synchronization with respect to the ratio between random uniform IC and space homogeneous IC in the fully connected network. The figure shows that increasing the space dispersion in IC increase the coupling strength threshold.

3.2 *Unidirectionally coupled ring network*

For the unidirectionally ring connected network, the system reads as:

$$\begin{cases} \varepsilon u_{it} = d_u \Delta u_i - u_i^3 + 3u_i - v_i - g_n \sum\limits_{j=1, j\neq i}^{n} (u_i - u_{i+1}) \\ v_{it} = a u_i - b v_i + c(x) \end{cases} \qquad i = \overline{1,n}, \tag{3.4}$$

where g_n is the constant coupling strength between each pair of nodes corresponding to an edge in the graph. We comment hereafter the numerical simulations illustrated in figures 10-11 below. The table 2

IC	$c(x)=0$	$c(x)\neq 0$
H	$1.33\times 10^{-3}n^2-0.00027n+0.014$	$1.1\times 10^{-3}n^2-0.00492n+0.0148$
S+H	$9.4\times 10^{-4}n^2+0.00063n+0.03$	$1.7\times n^2+0.0005n+0.0187$
RU1+H	$2.55\times 10^{-4}n^2-0.00083n+0.023$	$15.73\times 10^{-5}n^2-0.0000729n+0.0097$
RU2+H	$3\times 10^{-4}n^2-0.0015n+0.0378$	$1.13\times 10^{-4}+0.003095n+0.004696$
S	$1.17\times 10^{-3}n^2-0.00217n+0.016$	$2.25\times 10^{-3}-0.0088n+0.021$
RU2	$2.5\times 10^{-3}n^2-0.0025n+0.025$	$6.46\times 10^{-4}n^2-0.00117n+0.0197$

Table 2. **Unidirectionally ring network.** Laws of synchronization threshold values with respect to the number of nodes in unidirectionally networks. We choose different kind of initial conditions leading to several patterns. All the simulations show the emergence of a quadratic law of synchronization. The abbreviations are the following: IC= initial conditions, H= space homogeneous, S= spirals, RU1= random uniform law on $[0,1]$, RU2= random uniform law on $[-1,1]$, S+H= half of S and half of H. $c(x)\neq 0$ means $c(x)=0$ at center and $c(x)=1.1$ otherwise.

summarizes the detailed heuristic laws found numerically.

- In figure 10, we present the evolution of the coupling strength value g_n needed for synchronization with respect to the number of nodes in the graph. For IC we choosethem as spirals and the other half as spatially homogeneous.. The number of nodes varies from 3 to 20, and we obtain an heuristic quadratic law in n^2. This is in good agreement with our theoretical results. We have also obtained the same heuristic laws as when we choose only spirals for IC or spirals and homogeneous or even with $c(x)$ non-constant function. Thus, the spatial effects induced by IC do not affect this heuristic law as already found on ODE's ring coupled networks.

- The figure 11 presents the evolution of the network, for $n=3$, when for each $x\in\Omega$, we choose IC $u_i(x,0)$ and $v_i(x,0)$, $i\in\{1,2,3\}$ as random uniform values in $[-1,1]$. Simulations show synchronization for a threshold value of $g_3\simeq 0.02$. They also show asymptotically three multiple spiral matched patterns.

REMARK 3.1 In general, for one single FHN RD system (with constant homogeneous coefficients), the solution will evolve toward homogeneous state in space. This means that in fact, the homogeneous in space solution is the asymptotic behavior for a large set of IC. To obtain spiral or other patterns, it is necessary to choose very specific IC. These specific IC lead to patterns which appear to be numerically locally stable: choosing IC close leads to analog solutions. These considerations have been discussed in more detail in [2–4] and a more systematic stability analysis is being investigated. The choice of these patterns or homogeneous states for synchronization is a result of our previous works in [2–4].

4. Conclusion

In this paper, we have studied the synchronization phenomenon for general networks of coupled reaction-diffusion systems. Assuming the existence of the global attractor which has been proved in a previous work, we obtained two main contributions. First, we found out theoretically threshold values for synchronization for general class of networks with linear coupling. In the case of fully connected networks and ring networks, computations lead to respectively, an inverse power law and a quadratic law for synchronization, regarding the number of nodes in the graph. Secondly, we have performed numerical simulations with various sets of initial conditions and studied numerically the spatial effects on synchronization and pattern formation. We have numerically exhibited heuristic laws for synchronization, which match with our theoretical results and do not depend on spatial heterogeneity. In future works we aim to extend this analysis to more realistic complex networks of reaction-diffusion systems.

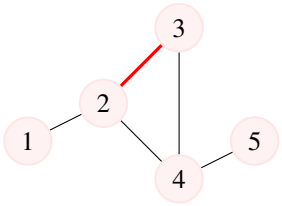

FIG. 1. Computation of the number α_{kl} in an example. The minimal path joining 1 and 2 is $P_{12} = 1-2$, $P_{13} = 1-2-3$, $P_{14} = 1-2-4$, $P_{15} = 1-2-4-5$, $P_{23} = 2-3$, $P_{24} = 2-4$,$P_{25} = 2-4-5$, $P_{34} = 3-4$, $P_{35} = 3-4-5$, $P_{45} = 4-5$. It follows that $\alpha_{23} = P_{13} + P_{23} = 2+1 = 3$.

REFERENCES

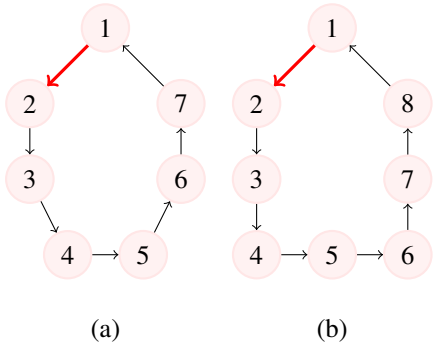

FIG. 2. Unidirectionally coupled ring. In panel a), the graph has an odd number of nodes, $n = 7$. There exists a unique minimal path joining each pair of nodes in the graph. For example, the computation of α_{12} is given by $\alpha_{12} = (1+2+3)+(2+3)+(3)$. The order of the computation follows from the counting of all the lengths of the minimal paths passing through the edge $(1,2)$, starting at 1,7 and 6. In panel b), the graph has an even number of nodes, $n = 8$. If the distance between two nodes is equal to $\frac{n}{2} = 4$, there exist two distinct minimal paths joining these nodes. For example, we can link node 1 and node 5 either by the path $1-2-3-4-5$ or by $1-8-7-6-5$. Therefore, we choose the path $1-2-3-4-5$ to connect nodes 1 and 5, whereas we choose the path $2-1-8-7-6$ to connect 2 and 6, and so on. Then computation of α_{12} is given by $\alpha_{12} = (1+2+3+4)+(2+3)+(3+4)$.

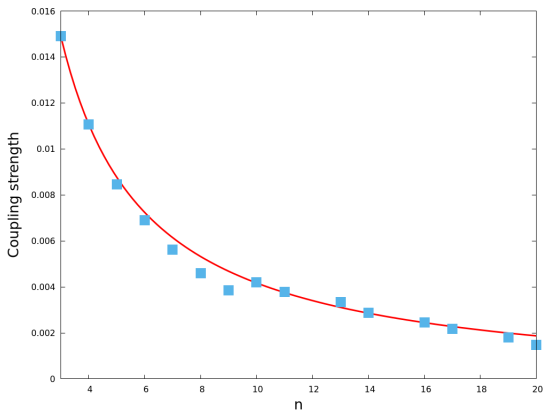

FIG. 3. **Fully connected network. Case $c(x) = 0$ with spiral and homogeneous IC.** Evolution of the coupling strength value g_n needed for synchronization with respect to the number of nodes, n in the graph for a fully connected network of type (3.3) with $c(x) = 0$, when n varies from 3 to 20. For initial conditions, we choose approximately 50% of spirals and 50% of homogeneous. The blue points represent the values obtained numerically, the red curve represents the function $g_n = \dfrac{0.046}{n} - 0.00043$. Thus, we obtain heuristically the widespread $\frac{1}{n}$ inverse power law which highlights the synchronization emergent property, see for example [17, 18].

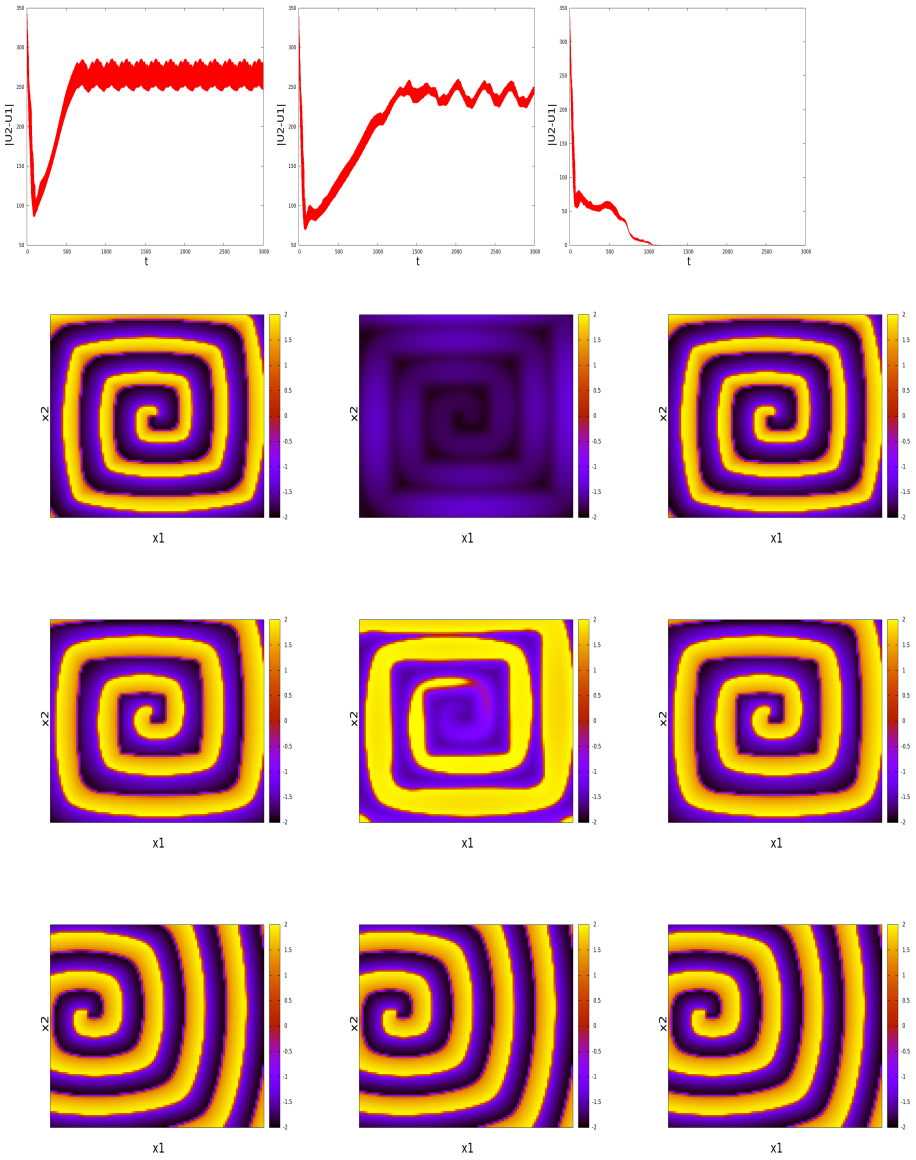

FIG. 4. **Fully connected network. Case $c(x) = 0$ with spiral and homogeneous IC.** Synchronization of a fully connected network (3.3) with $n = 3$, $c(x) = 0$. We choose two spirals and one homogeneous in space IC. We observe that the synchronization occurs for $g_3 \geqslant 0.015$. The first row represents, from left to right the synchronization error respectively between u_1 and u_2, for $g_3 = 0.01, 0.013, 0.015$. Since the two spirals have the same IC, by symmetry, the synchroniration error between u_3 and u_2 will be the same. Rows 3, 4 and 5 illustrate, respectively from left to right the isovalues of u_1, u_2 and u_3 for all $x = (x_1, x_2) \in \Omega$ at time 2500. Each row, form row 2 to row 4 corresponds respectively to the following values of g_3: 0.01, 0.013, 0.015. Asymptotically, the three subsystems evolve with the same spiral patterns.

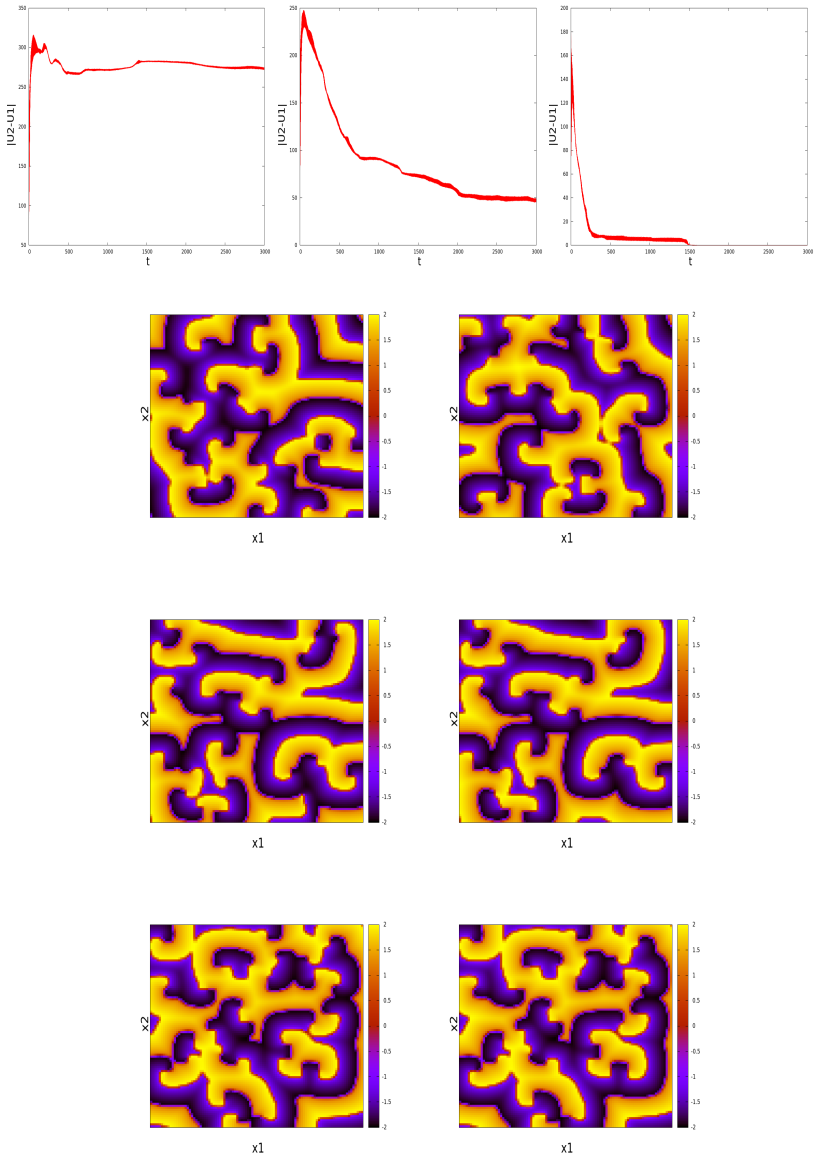

FIG. 5. **Fully connected network. Case $c(x) = 0$ with random uniform IC in $[-1,1]$.** Synchronization of a fully connected network (3.3) with $n = 3$, $c(x) = 0$. We choose random IC as follows: for each $x \in \Omega$, we choose $u_i(x,0)$ and $v_i(x,0)$, $i \in \{1,3\}$ as random uniform values in $[-1,1]$. IC $u_2(x,0)$ and $v_2(x,0)$ are choosen equal to 0. We observe that the synchronization occurs for $g_3 \geqslant 0.014$. Row 1 represents, from left to right the synchronization error between u_1 and u_2 for g_3= $0.001, 0.005, 0.014$. Each row, from row 2 to row 4, corresponds respectively to the following values for g_3: $0.001, 0.005, 0.014$. For rows $2,3,4$, we represent from left to right the isovalues of u_1 and u_2 for all $x = (x_1, x_2) \in \Omega$ at time 2500. By symmetry u_1 and u_3 are equal and we do not represent u_3. Asymptotically, the three subsystems evolve with the same patterns.

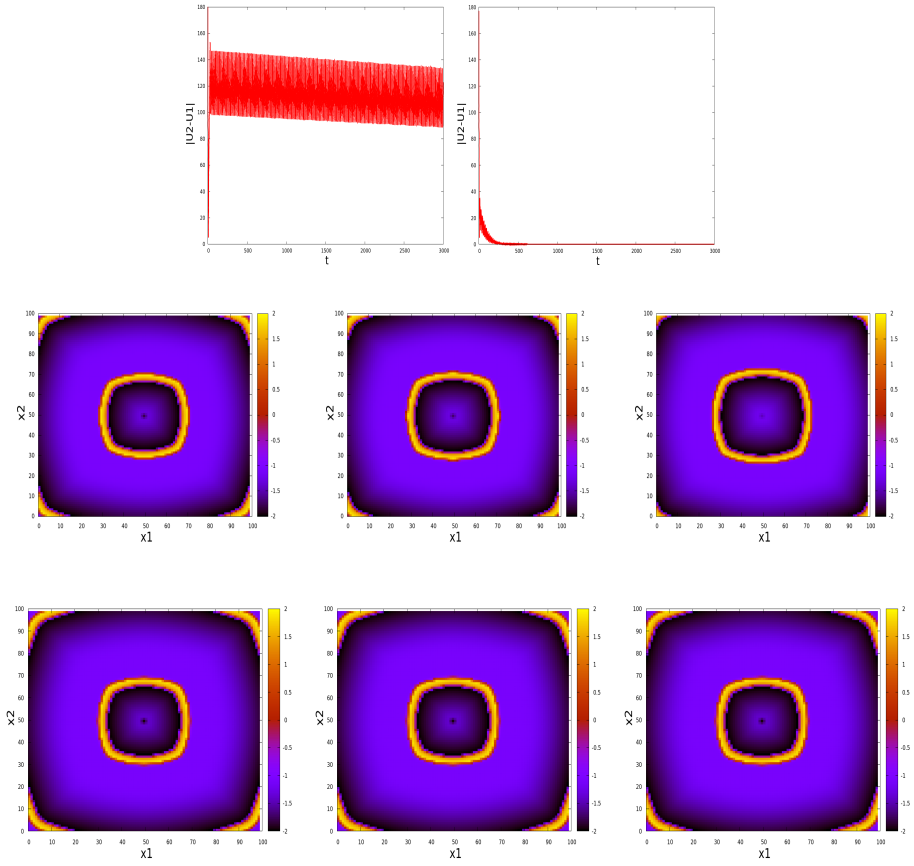

FIG. 6. **Fully connected network. Case $c(x) \neq 0$ with distinct space-homogeneous IC values.** Synchronization of a fully connected network (3.3) with $n = 3$, and $c(x) = 0$ if x is in a small neighborhood of the center of Ω, $c(x) = -1.1$ otherwise. Since the FHN ODE system may be either excitable or oscillatory, choosing such a $c(x)$ function, allows the generation of propagating periodic pulses starting at $(0,0)$, see [1]. For IC, we choose three distinct space-homogeneous values. The synchronization occurs for $g_3 \geqslant 0.001$. Row 1 represents, from left to right the synchronization error between u_1 and u_2 for $g_3 = 5 \times 10^{-6}$ and $g_3 = 5 \times 10^{-3}$. Row 2 illustrates respectively from left to right the isovalues of u_1, u_2 and u_3 for all $x = (x_1, x_2) \in \Omega$ at time 2500 for $g_3 = 5 \times 10^{-6}$. Row 3 illustrates analog simulations for $g_3 = 5 \times 10^{-3}$. Asymptotically, the three subsystems generate matching propagating concentric rings. See also figure .

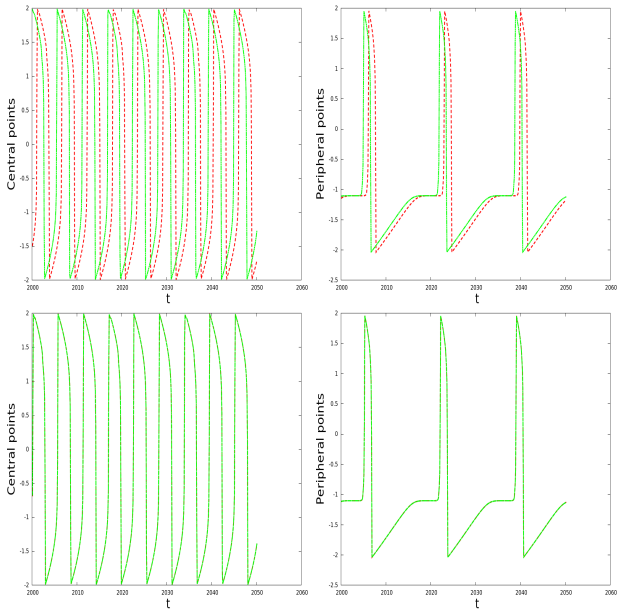

FIG. 7. **Fully connected network. Case $c(x) \neq 0$ with distinct space-homogeneous IC values.** Synchronization of a fully connected network (3.3) with $n = 3$, and $c(x) = 0$ if x is in a small neighborhood of the center of Ω, $c(x) = -1.1$ otherwise. Since the FHN ODE system may be either excitable or oscillatory, choosing such a $c(x)$ function, allows the generation of propagating periodic pulses starting at $(0,0)$, see [1]. For IC, we choose three distinct space-homogeneous values. The synchronization occurs for $g_3 \geqslant 5 \times 10^{-3}$. The first row corresponds to $g_3 = 5 \times 10^{-6}$ whereas the second one corresponds to $g_3 \geqslant 5 \times 10^{-3}$. The first column represents the time evolution of central cells $(u_i(50,50,t), i \in \{1,3\})$, whereas the second one represent the time evolution of peripheral cells $(u_i(50,99,t), i \in \{1,3\})$. The solid green line is for node one. The dashed red one is for node three. We observe that synchronization occurs for $g_3 = 0.0001$.

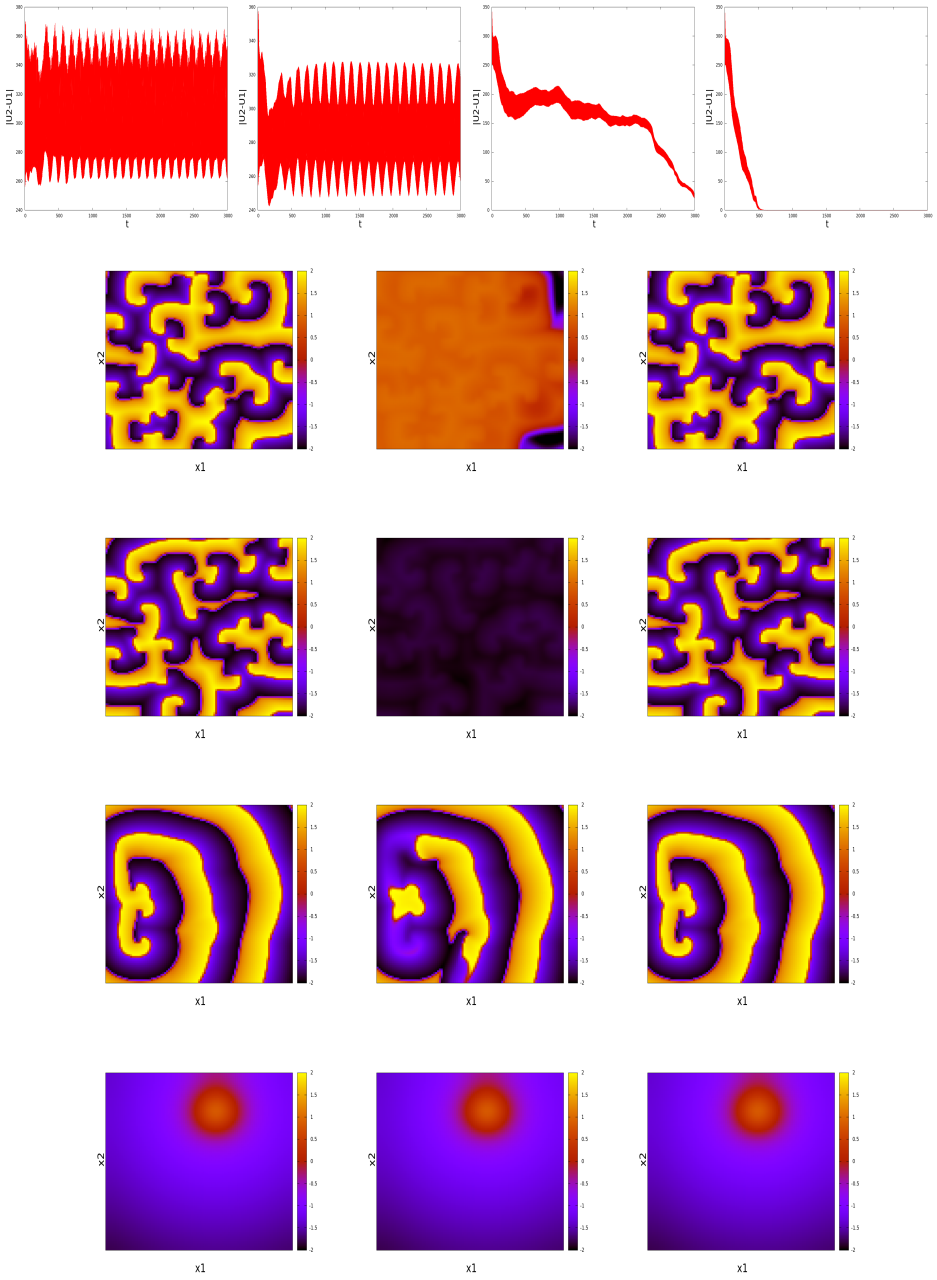

FIG. 8. **Fully connected network. Case $c(x) = 0$ with random uniform IC in $[-1,1]$.** Synchronization of a fully connected network (3.3) with $n = 3$, $c(x) = 0$. We choose random IC as follows: for each $x \in \Omega$, we choose $u_i(x,0)$ and $v_i(x,0)$, $i \in \{1,3\}$ as random uniform values in $[-1,1]$. $u_2(x,0)$ and $v_2(x,0)$ are set to 1. This is the only differnce with simulations shown in figure 5. We observe that the synchronization occurs for $g_3 \geqslant 0.015$. Rows 1 represents, from left to right the synchronization error between u_1 and u_2. Each row, from row 2 to row 4, corresponds respectively to the following values for g_3: $0.001, 0.005, 0.014$ and 0.015. For rows $2,3,4$, we represent from left to right the isovalues of u_1, u_2 and u_3 for all $x = (x_1,x_2) \in \Omega$ at time 2500. Asymptotically, the three subsystems evolve with the same patterns. Note however, that multiple spiral patterns have disappeared. This has to be linked with the lack of symmetry induced by setting $u_2(x,0)$ and $v_2(x,0)$ to 1.

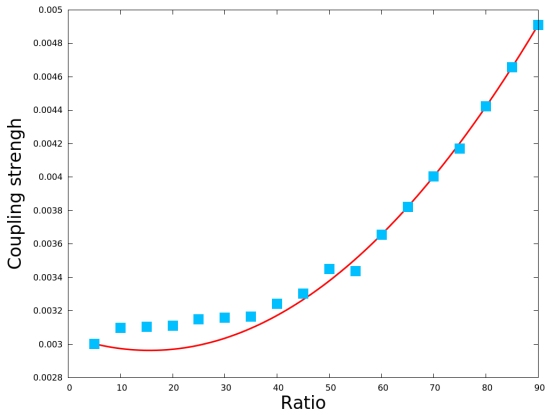

FIG. 9. Fully connected network. Evolution of the coupling strength value g_{20} needed for synchronization with respect to the ratio between random uniform IC and space homogeneous IC in the fully connected network. The blue points represent the values obtained numerically, the red curve represents the function $g_n(p) = 352 \times 10^{-9} p^2 - 11 \times 10^{-6} p + 0.00305$.

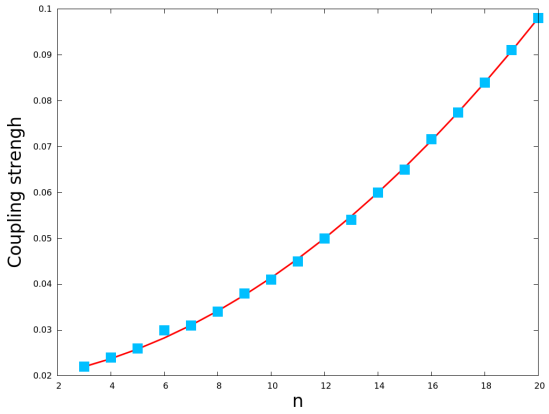

FIG. 10. **Unidirectionally ring network. Case $c(x) = 0$ with spiral and homogeneous IC.** Evolution of the coupling strength value g_n needed for synchronization with respect to the number of nodes, n in the graph of the unidirectionally ring network (3.4) with $c(x) = 0$, when n varies from 3 to 20. For IC, we choose approximately 50% of spirals and 50% of homogeneous. The blue points represent the values obtained numerically, the red curve represents the function $g_n = 0.000169935n^2 + 0.000562092n + 0.0187843$.

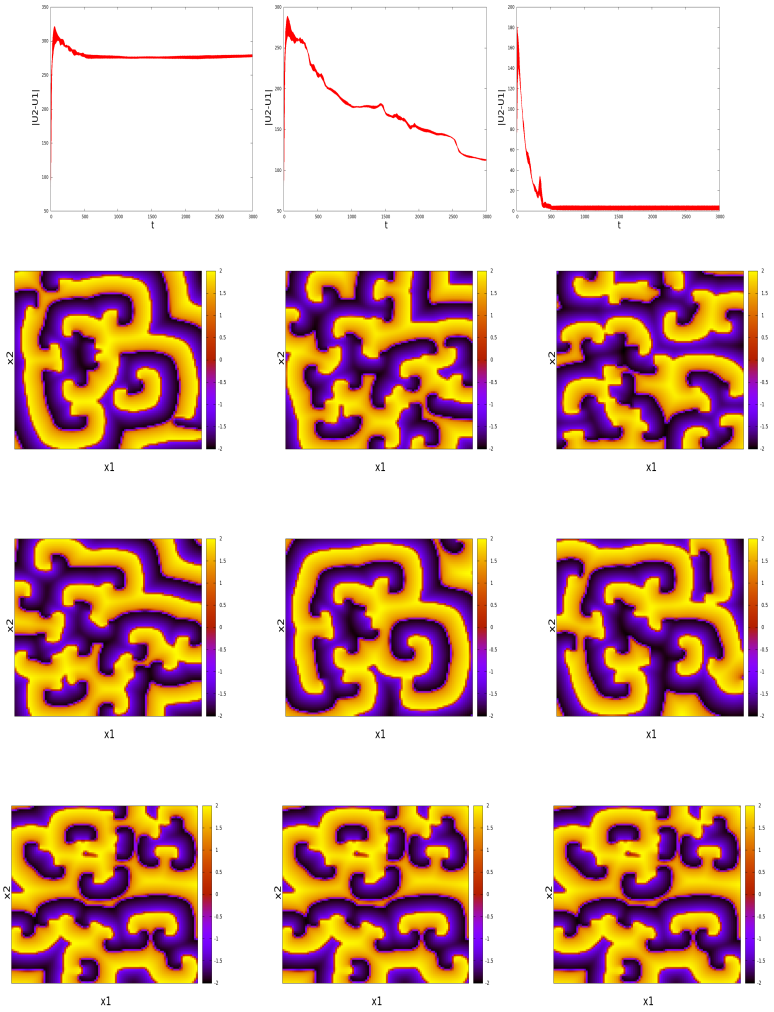

FIG. 11. **Unidirectionally ring network. Case $c(x) = 0$ with uniform random IC in $[-1,1]$.** Synchronization of a ring network (3.4) with $n = 3$, $c(x) = 0$. Random IC are obtained as follows: for each $x \in \Omega$, we $u_i(x,0)$ and $v_i(x,0)$, $i \in \{1,2,3\}$ as random uniform values in $[-1,1]$. We observe that the synchronization occurs for $g_3 \geqslant 0.02$. Each row, from up to down, corresponds respectively to the following values of g_3: $0.001, 0.005, 0.02$. The two first columns represent the synchronization error respectively between u_1 and u_2 and u_2 and u_3. The three others columns represent respectively from left to right the isovalues of u_1, u_2 and u_3 for all $x = (x_1, x_2) \in \Omega$ at time 3000. Asymptotically, the three subsystems evolve with multiple spirals matched patterns.

[1] B. AMBROSIO AND J-P. FRANÇOISE, *Propagation of Bursting Oscillations*, Phil. Trans. R. Soc. A, 367 (2009), p. 4863-4875.
[2] B. AMBROSIO AND M.A. AZIZ-ALAOUI, *Synchronization and control of coupled reaction-diffusion systems of the FitzHugh-Nagumo-type*, Comput. Math. Appl., 64 (2012), p. 934-943.
[3] B. AMBROSIO AND M.A. AZIZ-ALAOUI, *Network synchronization for generalized FitzHugh-Nagumo reaction diffusion systems*, ESAIM proc., 39 (2013), p. 15-24.
[4] B. AMBROSIO AND M.A. AZIZ-ALAOUI, *On the basin of attraction of patterns for the reaction-diffusion system of generalized FitzHugh-Nagumo type in ocillatory regime*, Acta Biotheoretica 64 (2016), p. 311-325.
[5] B. AMBROSIO, M.A. AZIZ-ALAOUI, V.L.E. PHAN, *Global attractor of complex networks of reaction-diffusion systems of Fitzhugh-Nagumo type*, Discrete and Continuous Dynamical Systems B, published on line.
[6] M. ARENA, A. DAZ-GUILERA, J. KURTHS, Y. MORENO, C. ZHOU, *Synchronizationin Complex Networks*, arXiv:0805.2976v3 (2008)
[7] M. ASLLANI, F. DI PATTI, D. FANELLI, ,Phys. Rev. E 86, 046105 (2012)
[8] M. ASLLANI, T. BIANCALANI, D. FANELLI, A.J. MCKANE, , Eur. Phys. J. B 86, 476 (2013)
[9] M. ASLLANI, J.D. CHALLENGER, F. S. PAVONE, L. SACCONI AND D. FANELLI, *The theory of pattern formation on directed networks*, Nat. Comm. 5 (2014) p. 4517-4525
[10] E. G. ANTZOULATOS, E.K. MILLER, *Increases in Functional Connectivity between Prefrontal Cortex and Striatum during Category Learning*, Neuron, 83 (1) (2014) p. 216225.
[11] M.A. AZIZ-ALAOUI, *Synchronization of Chaos*, Encyclopedia of Mathematical Physics, Elsevier, Vol. 5, (2006) p. 213-226.
[12] A. BARRAT, M. BARTHELEMY, A. VESPIGNANI, *Dynamical processes on complex networks*, Cambridge press, 2008.
[13] V.N. BELYKH, I. BELYKH, M. HASLER, *Connection graph stability method for synchronized coupled chaotic systems*, Physica D, 195 (2004), p. 159-187.
[14] I. BELYKH, V.N BELYKH, M. HASLER, *Sychronization in asymmetrically coupled networks with node balance*, Chaos 16, (2006), 015102.
[15] I. BELYKH, V.N BELYKH, M. HASLER, *Generalized connection graph method for synchronization in asymmetrical networks*, Physica D, 224 (2006), p. 42-51.
[16] E. CONWAY, D. HOFF, J. SMOLLER, *Large time behavior of solutions of systems of nonlinear reaction-diffusion equations*, SIAM J. Appl. Math. 35 (1978), p. 1-16.
[17] N. CORSON, M.A. AZIZ-ALAOUI, R. GHNEMAT, S. BALEV, C. BERTELLE, *Modeling the Dynamics of Complex Interaction Systems: from Morphogenesis to Control*, Internat. J. Bifur. Chaos, 22 (2012), 1250025.
[18] N. CORSON, M.A. AZIZ-ALAOUI, *Complex emergent properties in synchronized neuronal oscillations*, in M.A. Aziz-Alaoui and C. Bertelle (eds.): From System Complexity to Emergent Properties, Springer, (2009), p. 243-259.
[19] *Giulia Cencetti, Franco Bagnoli, Giorgio Battistelli, Luigi Chisci, Francesca Di Patti and Duccio Fanelli*, EPJB 90:9 (2017).
[20] S. CONTEMORI, FRANCESCA DI PATTI, DUCCIO FANELLI AND FILIPPO MIELE, *Multiple-scale theory of topology-driven patterns on directed networks*, PHYS. REV. E, 93 (2016), 032317.
[21] F. DORFLER AND F. BULLO, *On the Critical Coupling for Kuramoto Oscillators*, SIAM J. APPL. DYN. SYST., 10 (2011), P. 10701099.
[22] F. DORFLER AND F. BULLO, *Synchronization and Transient Stability in Power Networks and Nonuniform Kuramoto Oscillators* SIAM J. CONTROL OPTIM., 50 (2009), P. 16161642.
[23] J. FELL, N. AXMACHER, *The role of phase synchronization in memory processes*. NATURE REVIEWS NEUROSCIENCE 12 (2) (2011), P.105118.
[24] R. A. FITZHUGH, *Impulses and physiological states in theoretical models of nerve membrane*, BIOPHYSICAL JOURNAL. 1 (1961), P. 445-466.
[25] P. FRIES,*A mechanism for cognitive dynamics: neuronal communication through neuronal coherence* TICS 9 (10) (2005), P. 474-480.
[26] A. FRIEDMAN, *Partial Differential Equations of Parabolic Type*, DOVER EDITION, 2008.

[27] W. GERSTNER, W.M. KISTLER, R. NAUD AND L. PANINSKI, *Neuronal Dynamics* ,BIRKHAUSER, 2002.
[28] M. GOLUBITSKY AND I. STEWART, *The Symmetry Perspective* ,BIRKHAUSER, 2002.
[29] D. HENRY, *Geometric Theory of Semilinear Parabolic Equations*, SPRINGER, 1981.
[30] M.L. HINES AND N.T. CARNEVALE, *The NEURON Simulation Environment*, NEURAL COMPUTATION 9(1997), P. 1179-1209.
[31] A.L. HODGKIN AND A.F. HUXLEY, *A quantitative description of membrane current and its application to conduction and excitation in nerve*, J. PHYSIOL.117 (1952), P. 500-544.
[32] L. KOCAREV, Z. TASEV AND U. PARLITZ, *Synchronizing Spatiotemporal Chaos of Partial Differential Equations*, PRL, 79, (1997), P. 500-544.
[33] M. KRUPA, B. AMBROSIO AND M.A. AZIZ-ALAOUI, *Weakly coupled two-slowtwo-fast systems, folded singularities and mixed mode oscillations*, NONLINEARITY, 27 (2014), P. 1555-1574.
[34] O.A. LADYZENSKAJA, V.A. SOLONNIKOV AND N.N. URAL'CEVA, *Linear and Quasilinear Equations of Parabolic Type*, AM. MATH. SOC., PROVIDENCE, RHODE ISLAND, TRANSL. OF MATH. MONOGRAPHS 23, 1968.
[35] J. L. LIONS, *Quelques méthodes de résolution des problèmes aux limites non linéaires*, DUNOD, PARIS, 1969.
[36] M. MARION, *Finite Dimensionnal Attractors associated with Partly Dissipative Reaction-Diffusion Systems*, SIAM, J. MATH. ANAL. 20 (1989), P. 816-844.
[37] R.E. MIROLLO AND S.H. STROGATZ , *Synchronization of Pulse-Coupled Biological Oscillators*, SIAM J. AP. MATH,50(6), (1989), P. 1645-1662.
[38] X. MORA, *Semilinear Parabolic Problems define semiflows on C^k spaces*, TRANSACTIONS OF THE AMS, 278 (1983), P. 21-54.
[39] J. NAGUMO, S. ARIMOTO AND S. YOSHIZAWA, *An active pulse transmission line simulating nerve axon*, PROC. IRE. 50 (1962), P. 2061-2070.
[40] H. NAKAO AND A.S. MIKHAILOV, *Turing patterns in network-organized activator-inhibitor systems*, NAT. PHYS. 6 (2010), P. 544-550.
[41] H. NAKAO, *Complex Ginzburg-Landau equation on networks and its non-uniform dynamics*, EUR. PHYS. J. SPECIAL TOPICS 223 (2014), P 2411-2421.
[42] G.V. OSIPOV,J. KURTHS AND C. ZHOU, *Synchronization in Oscillatory Networks*, SPRINGER, (2007).
[43] H.G. OTHMER AND L.E. SCRIVEN, *Instability and Dynamic Pattern in Cellular Networks*, J. THEOR. BIOL. 32 (1971), P. 507-537.
[44] H.G. OTHMER AND L.E. SCRIVEN, , J. THEOR. BIOL. 43 (1974), P. 83-112.
[45] D. PAPO, J.M. BULDU, S. BOCCALETTI AND E. T. BULLMORE ,*Complex network theory and the brain*. PHIL. TRANS. R. SOC. B 369(2014):20130520.
[46] L. PECORA AND T. CARROLL,*Synchronization in chaotic systems*, PHYSICAL REVIEW LETTERS 64, (1990), P. 821824.
[47] C. S. PESKIN,*Mathematical Aspects of Heart Physiology*, COURANT INSTITUTE OF MATHEMATICAL SCIENCE, NEW YORK UNIVERSITY, NEW YORK, 1975.
[48] A. PIKOVSKY, M. ROSENBLUM AND J. KUTHS, *Synchronization*, CAMBRIDGE UNIVERSITY PRESS, (2001).
[49] F. A. RODRIGUES, T.K.DM. PERON, P. JI AND J. KUTHS, *The Kuramoto model in Complex Networks*, PHYSIC REPORTS, 610, (2016), P. 1-98.
[50] J. RAUCH AND J. SMOLLER, *Qualitative Theory of the FitzHugh Nagumo Equations*, ADVANCES IN MATHEMATICS, 27 (1978), P. 12-44.
[51] F. ROTHE, *Global Solutions to Reaction-Diffusion Systems*, SPRINGER-VERLAG, BERLIN, 1984.
[52] J. SMOLLER, *Shock Waves and Reaction-Diffusion Equations*, SPRINGER, 1994.
[53] A. SCHNITZLER AND J. GROSS, *Normal and pathological oscillatory communication in the brain*, NATURE REVIEWS NEUROSCIENCE 6 (4), (2005), P. 285296.
[54] W. SENN AND R. URBANCZIK, *Similar nonleaky integrate-and-fire neurons with instantaneous coupling always synchronize*, SIAM J. APPL. MATH 61(4), (2000) P. 11431155

[55] R. TEMAM, *Infinite-Dimensional Dynamical Systems in Mechanics and Physics*, SPRINGER, 1988.
[56] A. TURING, *The chemical basis of morphogenesis*, PHIL. TRANS. R. SOC. B, 237, (1952), P.37-72.
[57] Z. XU, *Synchronization of two discrete GinzburgLandau equations using local coupling*, INT. J. NONLINEAR SCI. 1, (2009), P. 1929.
[58] L. ZEMANOVÁ, C. ZHOU, J. KURTHS, *Structural and functional clusters of complex brain networks*, PHYSICA D 224 (2006), P. 202212.
[59] C. ZHOU, L. ZEMANOVÁ, G. ZAMORA, C.C. HILGETAG, J. KURTHS, *Hierarchical Organization Unveiled by Functional Connectivity in Complex Brain Networks*, PRL 97, 238103, (2006).